

## Molecular modeling studies on the active binding site of the blood–brain barrier choline transporter

Werner J. Geldenhuys,<sup>a,b</sup> Paul R. Lockman,<sup>a</sup> James H. McAfee,<sup>a</sup> Kevin T. Fitzpatrick,<sup>a</sup> Cornelis J. Van der Schyf<sup>a</sup> and David D. Allen<sup>a,\*</sup>

<sup>a</sup>*Department of Pharmaceutical Sciences, Texas Tech University Health Sciences Center,  
School of Pharmacy, Amarillo, TX 79106, USA*

<sup>b</sup>*Department of Pharmaceutical Chemistry, North West University, Potchefstroom 2520, South Africa*

Received 20 February 2004; revised 9 April 2004; accepted 10 April 2004

**Abstract**—The blood–brain barrier choline transporter may have utility as a drug delivery vector to the central nervous system. Surprisingly, this transporter has as yet not been cloned and expressed. We therefore initiated a 3D-QSAR study to develop predictive models for compound binding and identify structural features important for binding to this transporter. In vivo experimental data were obtained from in situ rat brain perfusion studies. Comparative molecular field analysis (CoMFA) and comparative molecular similarity index analysis (CoMSIA) methods were used to build the models. The best cross-validated CoMFA  $q^2$  was found to be 0.47 and the non-cross-validated  $r^2$  was 0.95. CoMSIA hydrophobic cross-validated  $q^2$  was 0.37 and the non-cross-validated  $r^2$  was 0.85. These models rendered a useful approximation for binding requirements in the BBB-choline transporter and, until such time as the cloned transporter becomes available, may have significant utility in developing a predictive model for the rational design of drugs targeted to the brain.

© 2004 Elsevier Ltd. All rights reserved.

### 1. Introduction

For drugs that act in the central nervous system (CNS), a major rate-limiting step for uptake into the brain is passage through the blood–brain barrier (BBB). This is notable for hydrophilic compounds, for which the BBB is essentially impermeable.<sup>1–3</sup> Anatomically the BBB is comprised of brain capillary endothelial cells connected by tight junctions that circumferentially surround the endothelial cell margin and is responsible for preventing/retarding the passage of hydrophilic compounds into the CNS.<sup>4,5</sup> Numerous methods have been investigated to increase the delivery of drugs to the CNS. These methods include strategies to increase a drugs' lipid solubility by attachment of hydrophobic groups (e.g., adamantane moiety) or deletion of hydrophilic groups from the drug molecule. However, drug modification can result in drug inactivation via altered pharmacokinetics or structural

inability to bind to the required receptor.<sup>6</sup> An alternative option to bypass the BBB is utilizing a native nutrient transporter located at the barrier interface. This report specifically addresses the exploitation of the BBB-choline transporter as a drug delivery vector for compounds with a charged quaternary ammonium moiety.<sup>2,7</sup> This transporter is responsible for transporting choline, a charged cation, into the CNS where it acts as precursor for the neurotransmitter acetylcholine and as an essential component of membrane phospholipids such as phosphatidylcholine.<sup>8</sup> Utilizing this transporter could enable drugs to enter the brain in pharmacologically significant amounts.<sup>5</sup> Pharmacological applications of using the choline transporter for drug delivery to the CNS may include treatment strategies for Alzheimer's disease, hypoxia/ischemia after stroke or traumatic brain injury, and tobacco smoking-cessation.<sup>6</sup>

Surprisingly the BBB-choline transporter has not yet been cloned and expressed,<sup>2</sup> a fact that gave impetus to our interest in studying the requirements for ligand-transporter binding in this system using a combination of empirical and theoretical methodologies, such as those reported in this study. Previous literature reports

**Keywords:** Choline; Transport; Blood–brain barrier; Molecular modeling.

\* Corresponding author. Tel.: +1-806-356-4015x286; fax: +1-806-356-4034; e-mail: [david.allen@ttuhsc.edu](mailto:david.allen@ttuhsc.edu)

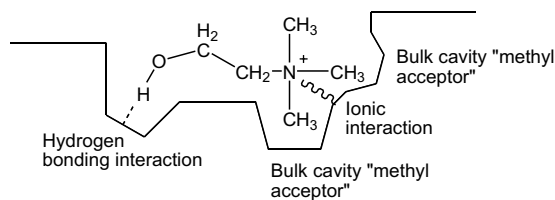


**Figure 1.** Theoretical rendering of the choline binding site in the choline transporter.<sup>2,6</sup>

suggest a number of structural requirements for the choline transporter binding site and we<sup>2,6</sup> have recently proposed a model for such interaction (Fig. 1). Briefly, the model provides for a primary interaction between a quaternary nitrogen moiety and a complementary binding site. In addition, a hydrogen bonding site, which displays significant restriction, is proposed. For instance, replacement of the hydrogen bond donor (hydroxyl) group with a methyl group, leads to a considerable decrease in affinity for the transporter. The distance between the quaternary nitrogen and the

hydroxyl group in potential ligands for the choline transporter binding site also has been found to be limited to approximately 3.26–3.30 Å.

In the present study, 3D-QSAR methods have been carried out to elucidate structural requirements for choline transporter binding. The information gleaned from this study predicts structural requirements for choline transporter ligands, thereby contributing to the knowledge required to design ligands for the utilization of this transporter as a drug delivery vector.

## 2. Methods

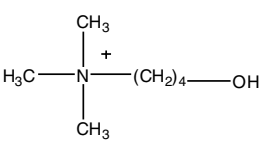
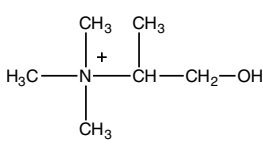
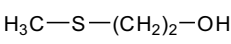
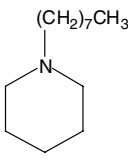
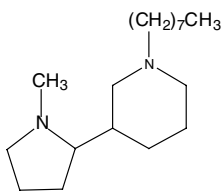
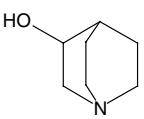
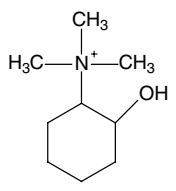
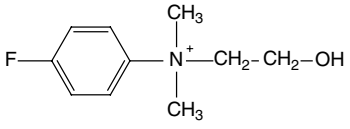
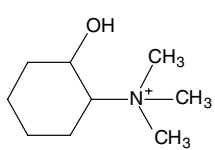
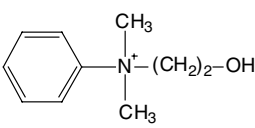
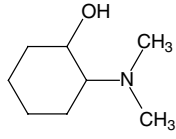
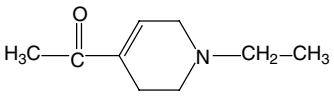
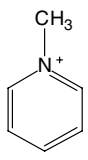
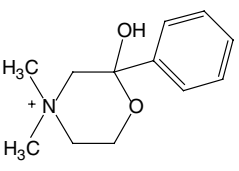
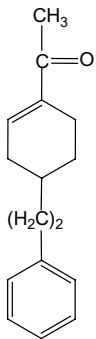
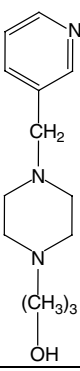
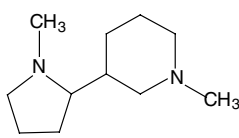
### 2.1. Structure building

Structures (Table 1) used in the study were built using SYBYL 6.91 (Tripos) molecular modeling software on a silicon graphics Octane computer. All molecules were

**Table 1.** Structures of compounds used in this study, listed with brain [<sup>3</sup>H]-choline uptake reduction  $K_i$  (μM) values obtained from in situ brain perfusion studies<sup>9</sup>

Compound	$K_i$	Compound	$K_i$
$\begin{array}{c} \text{(CH}_2\text{)}_7\text{CH}_3 \\   \\ \text{CH}_3\text{—N}^+\text{—CH}_2\text{—CH}_2\text{—OH} \\   \\ \text{CH}_3 \end{array}$	2.1	$\begin{array}{c} \text{(CH}_2\text{)}_5\text{CH}_3 \\   \\ \text{H}_3\text{C—N}^+\text{—CH}_2\text{—CH}_2\text{—OH} \\   \\ \text{CH}_3 \end{array}$	2.3
$\begin{array}{c} \text{CH}_3 \\   \\ \text{H}_3\text{C—N—CH}_2\text{—CH}_2\text{—OH} \end{array}$	21	$\begin{array}{c} \text{(CH}_2\text{)}_3\text{CH}_3 \\   \\ \text{H}_3\text{C—N}^+\text{—CH}_2\text{—CH}_2\text{—OH} \\   \\ \text{CH}_3 \end{array}$	40
$\begin{array}{c} \text{CH}_3 \\   \\ \text{H}_3\text{C—N}^+\text{—CH}_2\text{—CH}_2\text{—OH} \\   \\ \text{CH}_3 \end{array}$	42	$\begin{array}{c} \text{CH}_2\text{CH}_3 \\   \\ \text{H}_3\text{C—N}^+\text{—CH}_2\text{—CH}_2\text{—OH} \\   \\ \text{CH}_3 \end{array}$	94
$\begin{array}{c} \text{CH}_3 \\   \\ \text{H}_3\text{C—S—CH}_2\text{—CH}_2\text{—OH} \\   \\ \text{H} \end{array}$	117	$\text{CH}_3\text{—NH—CH}_2\text{—CH}_2\text{—OH}$	127
$\begin{array}{c} \text{CH}_3 \\   \\ \text{H}_3\text{C—N}^+\text{—CH}_2\text{—CH}_2\text{—CH}_2\text{—OH} \\   \\ \text{CH}_3 \end{array}$	162	$\begin{array}{c} \text{(CH}_2\text{)}_2\text{CH}_3 \\   \\ \text{CH}_3\text{—N}^+\text{—CH}_2\text{—CH}_2\text{—OH} \\   \\ \text{CH}_3 \end{array}$	190
$\begin{array}{c} \text{CH}_3 \quad \text{CH}_3 \\   \quad   \\ \text{H}_3\text{C—N}^+\text{—CH}_2\text{—CH—OH} \\   \\ \text{CH}_3 \end{array}$	200	$\text{H}_2\text{N—CH}_2\text{—CH}_2\text{—OH}$	903
$\begin{array}{c} \text{CH}_2\text{CH}_3 \\   \\ \text{H}_3\text{CH}_2\text{C—N}^+\text{—CH}_2\text{—CH}_2\text{—OH} \\   \\ \text{CH}_2\text{CH}_3 \end{array}$	1903	$\begin{array}{c} \text{CH}_3 \\   \\ \text{H}_3\text{C—N}^+\text{—CH}_2\text{—CH}_3 \\   \\ \text{CH}_3 \end{array}$	4698

Table 1 (continued)

Compound	$K_i$	Compound	$K_i$
	>10,000		>10,000
	>10,000		
	32		45
	200		574
	737		5369
	>10,000		>10,000
	>10,000		>10,000
	384		495
	>10,000		>10,000

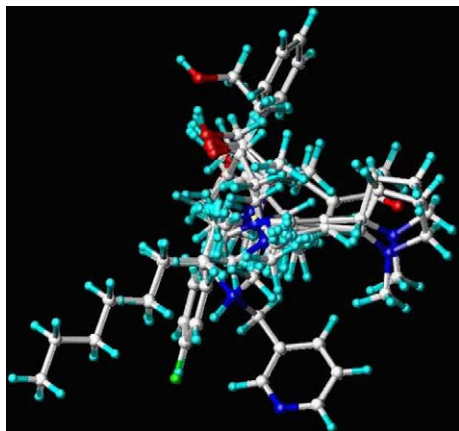


**Figure 2.** Alignment of compounds used to create the 3D-QSAR models.

energy minimized for CoMFA and CoMSIA analysis by systematically searching for lowest energy conformations by rotating bonds in  $10^\circ$  increments followed by energy minimization.

## 2.2. Molecular alignment

All compounds were aligned manually using the FIT ATOMS function in SYBYL (Fig. 2), by superimposing the cationic N-atom, the  $\alpha$ -carbon adjacent to the nitrogen atom and the hydroxyl group.

## 2.3. 3D-QSAR study

The CoMFA analysis was carried out using standard SYBYL/QSAR routine. CoMFA grid spacing was 2.0 Å in the *X*, *Y*, and *Z* directions, and grid regions were automatically generated by the CoMFA routine to encompass all molecules with an extension of 4.0 Å in each direction. An  $sp^3$  carbon for measuring steric interactions and a charge of +1.0 to explore electrostatics were used as probes to generate the interaction energies at each lattice point, with a default energy cutoff at 30 kcal/mol. Partial least squares (PLS) (cross-validated and non-cross-validated) regression analyses were performed from the resulting field. Column filtering (2.0 kcal/mol) was also investigated to see if such an approximation would result in improved  $q^2$  values. These relative contributions were represented as a 3D coefficient map with favored 80% steric (in green) and electrostatic (in blue) effects and the 20% disfavored steric (in yellow) and electrostatic effects (in red). The green colored areas of the map indicate where sterically bulky groups may enhance interaction affinity. The blue color indicates regions where electronegative groups have increased binding affinity.

## 2.4. Animals

Male Fischer-344 rats (220–330 g) were obtained from Charles River Laboratories, Inc. (Wilmington,

MA). All studies were done in accordance with the NIH guide for the care and use of laboratory animals, and were approved by the Animal Care and Use Committee of Texas Tech University Health Sciences Center.

## 2.5. In situ brain perfusion technique

Uptake of [ $^3\text{H}$ ]-choline into brain was assessed using the in situ rat brain perfusion technique<sup>9</sup> with modifications described.<sup>10,11</sup> Briefly in this study, short perfusions of 60 s were used to determine brain uptake of [ $^3\text{H}$ ]-choline. Once uptake values were calculated, subsequent experiments evaluated the inhibition of [ $^3\text{H}$ ]-choline brain uptake by 250  $\mu\text{M}$  of the test compounds.

## 2.6. Radiochemicals

[ $^{14}\text{C}$ ]-Sucrose (4.75 mCi/mmol) and [ $^3\text{H}$ ]-choline (79.2 Ci/mmol, >98% purity) were obtained from Dupont-New England Nuclear. In each experiment, [ $^3\text{H}$ ]-choline was dried prior to being dissolved in perfusion buffer to remove volatile tritium contaminants including [ $^3\text{H}$ ]- $\text{H}_2\text{O}$ .

## 2.7. Perfusion procedure

Rats were anesthetized with sodium pentobarbital (50 mg/kg intraperitoneal). A PE-60 catheter filled with heparinized saline (100 U/mL) was placed into the left common carotid artery after ligation of the left external carotid, occipital, and common carotid arteries. Common carotid artery ligation was accomplished caudally to the catheter implantation site. The pterygopalatine artery was left open during the experiments.<sup>11</sup> Rat rectal temperature was monitored and maintained at 37 °C by a heating pad connected to a feedback device (YSI Indicating Controller, Yellow Springs, Ohio). The catheter to the left common carotid artery was connected to a syringe containing buffered physiologic perfusion fluid (containing [in mM]: NaCl 128,  $\text{NaPO}_3$  2.4,  $\text{NaHCO}_3$  29.0, KCl 4.2, CaCl 1.5,  $\text{MgCl}_2$  0.9, and D-glucose 9) with 1  $\mu\text{Ci/mL}$  [ $^3\text{H}$ ]-choline and 0.3  $\mu\text{Ci/mL}$  [ $^{14}\text{C}$ ]-sucrose (to determine vascular volume). Perfusion fluid was filtered and warmed to 37 °C, and gassed with 95%  $\text{O}_2$  and 5%  $\text{CO}_2$ . Immediately prior to perfusion, the pH and osmolarity of this solution were  $\approx 7.35$  and 290 mOsm, respectively. The perfusion fluid was infused into the left carotid artery with an infusion pump for a period of 60 s at 10 mL/min (Harvard Apparatus, South Natick, MA, USA). This perfusion rate was selected to maintain a carotid artery pressure of  $\sim 120$  mmHg.<sup>9</sup> After the 60 s perfusion with [ $^3\text{H}$ ]-choline and its unlabeled analog, the perfusion fluid was changed immediately to tracer-free perfusion fluid for 15 s to wash out residual [ $^3\text{H}$ ]-choline, which had not been taken up into brain.<sup>11</sup>

Inhibition of [ $^3\text{H}$ ]-choline brain uptake was determined by the inclusion of unlabeled choline or

choline analog in the perfusion fluid. Structures of the compounds evaluated are shown in Table 1. To determine  $K_i$ , compounds were evaluated at initial concentrations of 250  $\mu\text{M}$ , unless specifically stated otherwise, using the method described previously<sup>12</sup> and detailed below.

Rats were decapitated and cerebral samples obtained as previously described.<sup>11</sup> Briefly, the brain was removed from the skull, and the perfused cerebral hemisphere dissected on ice after removal of the arachnoid membrane and meningeal vessels. Brain regions were placed in scintillation vials and weighed. In addition, two 50  $\mu\text{L}$  aliquots of the perfusion fluid were transferred to a scintillation vial and weighed. The brain and perfusion fluid samples were then digested overnight at 50 °C in 1 mL of 1 M piperidine solution. Ten mL of Fisher Chemical scintillation cocktail (Beckman, Fullerton, CA, USA) was added to each vial and the tracer contents assessed by dual-label liquid scintillation counting. Dual labeled scintillation counting of brain and perfusate samples was accomplished with correction for quench, background and efficiency.

Brain uptake of [ $^3\text{H}$ ]-choline was determined by calculation of a single time point blood-to-brain transfer coefficient ( $K_{in}$ ) as previously described<sup>9,13</sup> from the following relationship:

$$K_{in} = [C_{tot} - V_v C_{pf}] / (C_{pf} / T) \quad (1)$$

where  $C_{tot} = C_{br} + C_{vas}$ , the sum of the amount of choline remaining in the perfusate in the blood–brain vessels and the amount of choline that had penetrated into the brain. Cerebral vascular volume and cerebral perfusion flow rate were determined in separate experiments as previously described,<sup>6</sup>  $C_{pf}$  is the perfusion fluid concentration of tracer choline and  $T$  is the net perfusion time with the assumption that uptake is linear.

Apparent cerebrovascular permeability surface-area product (PA) was determined using the following relationship:

$$PA = F \ln(1 - k_{in} / F) \quad (2)$$

where  $F$  is the cerebral blood flow determined for each region of the brain from the uptake of [ $^{14}\text{C}$ ] diazepam according to the method of Momma et al.<sup>14</sup>

An apparent inhibition constant ( $K_i$ ) for choline and its choline analogs was determined<sup>12</sup> from the equation:

$$[(PA_o - K_D) / (PA_i - K_D)] = 1 + C_i / K_i \quad (3)$$

assuming competitive kinetics where  $PA_o$  is the [ $^3\text{H}$ ]-choline PA in the absence of competitor,  $PA_i$  is the [ $^3\text{H}$ ]-choline PA in the presence of inhibitor, and  $C_i$  is the perfusate concentration of inhibitor. Apparent  $K_i$  is defined as the inhibitor concentration that reduces saturable brain [ $^3\text{H}$ ]-choline influx by 50% at tracer choline concentration ( $C_{pf} \ll K_m$ ) and in the absence of other competing compounds. Previously, we demonstrated competition at the BBB-choline transporter with a 0.25–12.5  $\mu\text{M}$  concentration range of hemicholinium-3, the defining substrate for choline transport systems.<sup>11</sup>

### 3. Results and discussion

The delivery of drugs to CNS is limited by the drugs' physicochemical properties as well as the anatomical selectivity of the BBB. Drug uptake in CNS may be improved through chemical modifications of ligands or by the exploitation of native nutrient transporters such as the choline transporter as vectors. In this study we derived a 3D-QSAR model of the BBB-choline transporter, a possible BBB CNS drug vector. CoMFA and CoMSIA techniques were employed to gain insight into the structural requirements for compounds that bind to the transporter, as well as to derive predictive models for future drug design.

Results of CoMFA and CoMSIA analyses are shown in Tables 2 and 3, respectively. We developed two models, with the first consisting of 42 compounds, and the second (consisting of 33) from which outliers were removed to improve model predictability. The selection of the 33 compounds for the second model was based on consistent manual elimination in the annotation graph as displayed with the CoMFA model in SYBYL. For the first model, a cross-validated  $q^2$  of 0.395 was observed, which improved when column filtering of 2.0 kcal/mol was applied to give a final  $q^2$  of 0.425. A non-cross-validated  $r^2$  of 0.884 was observed for this model. Steric and electrostatic contributions were calculated to be 64% and 36%, respectively, suggesting that steric aspects for the cationic compounds are of para-

**Table 2.** Summary of CoMFA PLS analysis

Model	$q^2$	S.E.P.	Components	$r^2$	S.E.E.	Steric	Electrostatic
1	0.425 <sup>a</sup>	0.834	2	0.884	0.395	0.641	0.359
2	0.471 <sup>a</sup>	0.916	6	0.955	0.266	0.725	0.275

S.E.P.=Standard error of prediction; S.E.E.=standard error of estimate.

<sup>a</sup> Column filtering of 2 kcal/mol.

**Table 3.** Summary of CoMSIA PLS analysis

Model	$q^2$	S.E.P.	Components	$r^2$	S.E.E.
1	0.373 <sup>a</sup>	0.870	2	0.850	0.449
2	0.405 <sup>a</sup>	0.889	1	0.887	0.424

S.E.P.=Standard error of prediction; S.E.E.=standard error of estimate.

<sup>a</sup> Column filtering of 2 kcal/mol.

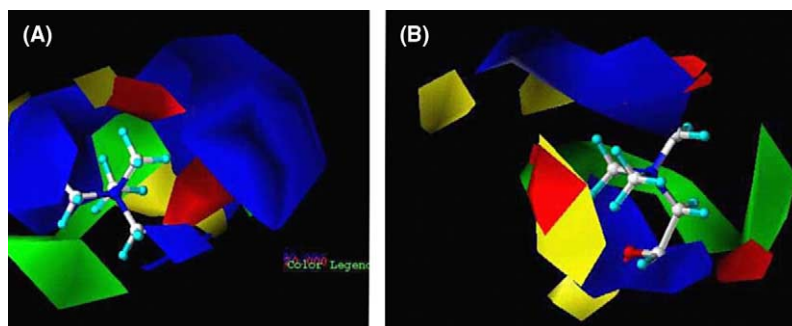


**Figure 3.** Contour maps of model 1 (A), and model 2 (B) CoMFA analysis. Steric fields are shown where green areas indicate regions where bulky substituents can be accommodated in a sterically favorable way and yellow unfavorable. Electrostatic fields are shown where blue areas would favorably accommodate cationic groups. Cationic interactions in red areas would be unfavorable. Choline is shown docked in the model.

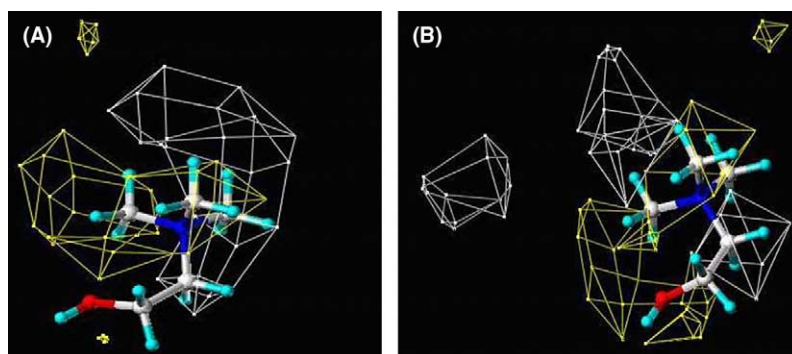
mount importance for adequate transporter binding. To determine if this model could be improved, we developed model 2, with fewer compounds. The cross-validated  $q^2$ -value improved from 0.395 to 0.430. With column filtering again set at 2.0 kcal/mol, this model was further improved to give a final model with a  $q^2$  of 0.471. The resulting non-cross-validated  $r^2$  improved from that of the previous model (0.884), to 0.955.

Figure 3 shows CoMFA contour plots of models 1 and 2. The green contours represent regions of high steric tolerance (80% contribution); while yellow contours represent regions of unfavorable steric interaction (20% contribution). Electrostatic contours are shown in blue and red, respectively. Blue contours represent those regions where positively charged groups would enhance activity (80% contribution) and the red region where negatively charged groups would enhance activity (20% contribution). In Figure 3A a green area surrounds the alkyl chain-segment of choline, as well as an area near the *N*-methyl groups. This area indicates a region where attachment of bulky groups would sterically complement the interaction between ligand and choline transporter. The same green 'band' is also seen in Figure 3B, suggesting a commonality between these two models. Figure 3A and B show a large ('favorable') blue area surrounding the cationic nitrogen, as would be expected for a cationic transporter, indicating the region where

the presence of positively charged substituents would be predicted to improve activity.

Figure 4 shows the results of CoMSIA hydrophobic field analyses. Favorable hydrophobic fields are indicated by yellow contours and unfavorable regions are indicated by white contours. The first model (Fig. 4A) shows primarily two areas surrounding the cationic nitrogen of choline. The white areas show where more hydrophilic substituents on compounds would likely increase affinity for the choline transporter, while yellow areas show where the addition of hydrophobic substituents may increase a compound's affinity. The refined model 2, with fewer compounds, shows more clearly the location of a number of areas that could be explored in the design of drugs that would have affinity for the choline transporter. For example, the *N*-methyl groups of choline are oriented toward areas that favor hydrophobic interactions.

As proof of concept for our model, we investigated the interaction of the '*cis*' and '*trans*' cyclic analogs of choline with the choline transporter. These geometric isomers were found to exhibit widely divergent choline transporter affinities (experimentally determined  $K_i$  values reported in Fig. 5). The '*cis*' cyclic analog displays a much higher affinity (574  $\mu$ M) for the transporter than does the '*trans*' cyclic analog (>10,000  $\mu$ M). Figure 5 shows both of these compounds docked into the CoM-



**Figure 4.** Contour maps of the CoMSIA hydrophobic fields with model 1 (A), and model 2 (B). Areas that favor hydrophobic interactions are indicated by yellow and areas that disfavor hydrophobic interactions by white. Choline is shown docked into the model.



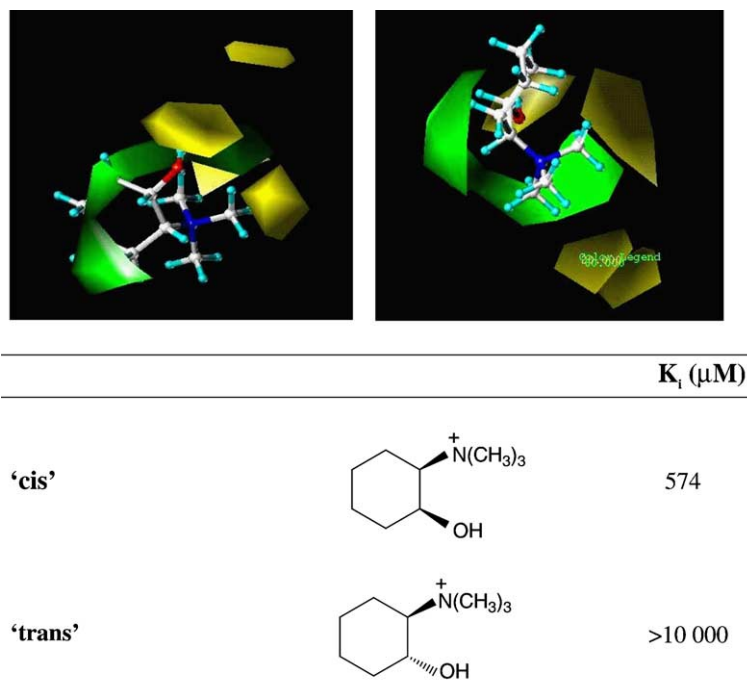


**Figure 5.** Steric contour map of the CoMFA analyses (model 2) with both the 'cis' and 'trans' cyclic analogs of choline docked into this model. The ring of the 'cis' analog extends into a favorable steric region, while the ring of the 'trans' analog extends toward a yellow 'unfavorable' region.

FA steric contour map of our model 2. The ring of the 'cis' analog is oriented toward an area where steric bulk is favored (green), while the ring of the 'trans' analog is oriented away from this favored area, and rather extends toward a sterically unfavorable (yellow) steric area. This finding might suggest why a pronounced difference in choline transporter affinity is seen for these two analogs.

A steric volume map of the BBB-choline transporter was built to further elucidate the general 3D shape of the transporter (Fig. 6). For this purpose, the inhibitors were categorized according to their activity at the transporter, which included (i) strongly active, with  $K_i < 30 \mu\text{M}$ ; (ii) active, with  $30 < K_i < 125 \mu\text{M}$ ; and (iii) inactive with  $K_i > 125 \mu\text{M}$ . This categorization indicates that the BBB-choline transporter binding site is larger

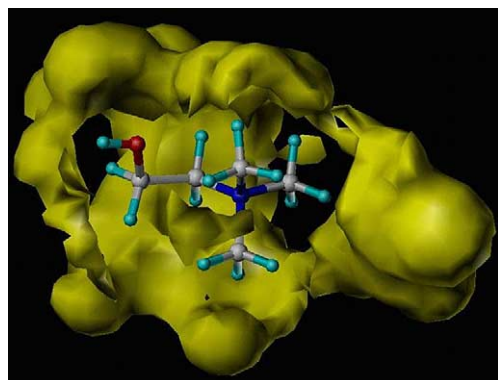


**Figure 6.** Steric volume map of the putative BBB-choline transporter active site cavity with choline shown docked inside and oriented according to the model shown in Figure 7.

than the choline molecule itself, suggesting that a diverse set of compounds may interact with the transporter. This finding is further supported by the diverse set of compounds that could be incorporated during the building of the CoMFA and CoMSIA models for the BBB-choline transporter (Fig. 7).

#### 4. Conclusion

The possibility of exploiting the BBB-choline transporter as a brain drug delivery vector led us to develop CoMFA and CoMSIA 3D-QSAR models that have afforded us to significantly improve and expand on our earlier model (shown in Fig. 1). These new models were built using empirical  $K_i$  data obtained from in situ rat brain perfusion experiments with a large and structurally diverse set of compounds. The molecular models have an excellent predictability value, which cross-validated at  $q^2 > 0.3$ . This predictability, however good, is

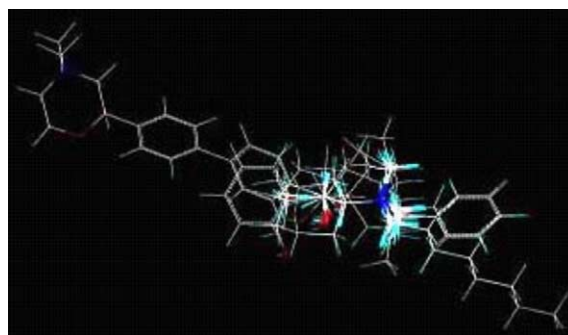


**Figure 7.** Alignment of compounds for the determination of the steric volume map.

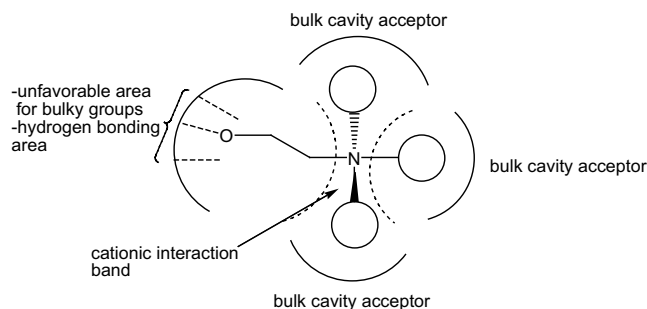


**Figure 8.** Theoretical rendering of the choline binding site in the choline transporter from the current and previous<sup>2,6</sup> studies.

limited by the compounds considered in this study and likely will improve even further as more compounds are synthesized, tested, and subjected to the modeling paradigm developed here. In their current form these models should have significant utility in: (1) identifying the structural binding requirements of the BBB-choline transporter and (2) providing a predictive model for the rational design of choline transporter ligands. Figure 8 summarizes the results from this study and those of previous<sup>2,6</sup> studies of the theoretical choline-transporter binding site.

## References and notes

1. Tamai, I.; Tsuji, A. *J. Pharm. Sci.* **2000**, *89*, 1371–1388.
2. Allen, D. D.; Lockman, P. R. *Life Sci.* **2003**, *73*, 1609–1615.
3. Clark, D. E. *Drug Discov. Today* **2003**, *8*, 927–933.
4. Malan, S. F.; Chetty, D. J.; Du Plessis, J. S. *Afr. J. Sci.* **2002**, *98*, 385–391.
5. Pardridge, W. M. *Nat. Rev. Drug Discov.* **2002**, *1*, 131–139.
6. Lockman, P. R.; Allen, D. D. *Drug Dev. Ind. Pharm.* **2002**, *28*, 749–771.
7. Allen, D. D.; Lockman, P. R.; Roder, K. E.; Dwoskin, L. P.; Crooks, P. A. *J. Pharmacol. Exp. Ther.* **2003**, *304*, 1247–1268.
8. Allen, D. D.; Smith, Q. R. *J. Neurochem.* **2001**, *76*, 1032–1041.
9. Takasato, Y.; Rapoport, S. I.; Smith, Q. R. *Am. J. Physiol.* **1984**, *247*, 484–493.
10. Smith, Q. R. *Pharm. Biotechnol.* **1996**, *8*, 285–307.
11. Allen, D. D.; Smith, Q. R. *J. Neurochem.* **2001**, *76*, 1–11.
12. Smith, Q. R.; Momma, S.; Aoyagi, M.; Rapoport, S. I. *J. Neurochem.* **1987**, *49*, 1651–1658.
13. Smith, Q. R.; Nagura, H.; Takada, Y.; Duncan, M. W. *J. Neurochem.* **1992**, *58*, 1330–1337.
14. Momma, S.; Aoyagi, M.; Rapoport, S. I.; Smith, Q. R. *J. Neurochem.* **1987**, *48*, 1291–1300.